Microchimica Acta (2020) 187: 488
https://doi.org/10.1007/s00604-020-04454-w

ORIGINAL PAPER

Accurate iron quantification in colloids and nanocomposites by a simple UV-Vis protocol

Miquel Torras[1] · Carlos Moya[1,2] · Gustavo A. Pasquevich[1,3] · Anna Roig[1]

Received: 16 March 2020 / Accepted: 14 July 2020 / Published online: 6 August 2020

Abstract

The selection and comparative study is reported of calibration curves to quantify iron by a simple UV-Vis protocol based on the formation of iron (III) chloride complexes. The reliability of each calibration curve was evaluated using statistical and analytical parameters. The robustness of each calibration curve using superparamagnetic iron oxide nanoparticles (SPIONs) of different sizes and surface functionalization is demonstrated . We have also evaluated the effect of the particle coating and estimated the minimum time to ensure the full oxidation of iron (II) to (III) in sample solutions. Results from UV-Vis are comparable with those obtained from ICP-OES and from other spectroscopic techniques to quantify the iron. We advocate the proposed protocol as a simple and non-expensive route to determine accurately the iron content in colloidal and nanocomposite iron-based materials.

Keywords Iron quantification · Iron oxide nanoparticles · Iron (III) chloride complexes · Ultraviolet–visible spectroscopy · Inductively coupled plasma optical emission

Introduction

SPIONs with magnetite (Fe_3O_4) or maghemite (γ-Fe_2O_3) crystal structures have been the focus of many research studies not only because of their interesting properties—high saturation magnetization at room temperature, low magnetic anisotropy, ease to make and functionalize, and good biocompatibility [1–3] but also for their wide scope of uses in many sectors from electronics to nanomedicine. Regarding biomedical applications, multiple examples can be found in the purification and isolation of proteins [4], in drug and gene delivery [5], hyperthermia therapy [6, 7], and as a contrast agents for magnetic resonance imaging (MRI) [8, 9]. Many chemical and physical properties describing these systems such as nanoparticle concentration, saturation magnetization, or specific relaxivity rely on a prior determination of the iron content [2, 10]. Thus, an accurate, reproducible, and accessible methodology to quantify iron is needed for a good understanding of these properties [10–12].

The most reliable techniques for iron determination are inductively coupled plasma optical emission (ICP-OES) and ultraviolet–visible spectroscopy (UV-Vis) [10–12]. Both techniques show accuracy values below 1% with UV-Vis being less sensitive. Note that the limit of detection (LOD) of iron for these techniques is $LOD_{ICP\text{-}OES} = 2{\cdot}10^{-6}$ g Fe/l and $LOD_{UV\text{-}VIS} = 3{\cdot}10^{-3}$ g Fe/l and the limit of quantification (LOQ) is $LOQ_{ICP\text{-}OES} = 7{\cdot}10^{-6}$ g and Fe/l, $LOQ_{UV\text{-}VIS} = 5{\cdot}10^{-3}$ g Fe/l [13–15]. Despite the higher LOD and LOQ values for UV-Vis, the technique offers interesting advantages. It is more economical in terms of equipment investment and running costs, easier to operate as self-user, and widely accessible in chemistry as well as materials science and physics labs. Besides, UV-Vis allows the determination of species with different oxidation states.

The sample preparation to quantify the iron by UV-Vis typically involves two steps. First, the addition of a concentrated acid solution to digest the sample and, second, the addition of a complexation agent to generate iron complexes that can be detected and quantified by UV-Vis [10–12]. The main drawback of using complexation agents is that dispersion of

Electronic supplementary material The online version of this article (https://doi.org/10.1007/s00604-020-04454-w) contains supplementary material, which is available to authorized users.

✉ Carlos Moya
cmoyaalv@ulb.ac.be

[1] Institut de Ciència de Materials de Barcelona (ICMAB-CSIC), Carrer dels Til·lers s/n Campus UAB, 08193 Bellaterra, Spain

[2] École Polytechnique de Bruxelles, Université libre de Bruxelles (ULB), Avenue F.D. Roosevelt 50, 165/64, 1050 Brussels, Belgium

[3] Instituto de Física La Plata (IFLP-CONICET), Universidad Nacional de la Plata, Diagonal 113 entre 63 y 64, 1900 La Plata, Argentina

values can be encountered due to the poor stability of these iron complexes. For example, potassium hexacyanoferrate (II) is a commonly used complexing agent that reacts with iron (III) yielding Prussian blue with a characteristic peak of around 600–700 nm [11, 12]. Due to its low solubility in aqueous media, it destabilizes fast, precipitating and hindering the reproducibility of the measurement. This can be solved with the use of an acid that itself forms iron complexes measurable by UV-Vis. A good example is a hydrochloric acid (HCl); the iron oxide digestion occurs in few minutes generating iron (III) chloride complexes with a sharp signal in UV-Vis range. The nature of these complexes depends on the HCl concentration giving extremely different UV-Vis spectra with band maxima in the 250–370 nm range [16–19]. Although these reactions have been already studied [16–19], the optimum HCl concentration for a consistent quantification of iron is still not well determined.

Here, we show a reliable quantification of iron by a universal UV-Vis protocol demonstrated by using four SPION colloidal dispersion of different sizes functionalized with widely employed organic molecules (citrate and oleic acid) as well as iron quantification in a composite of SPIONs attached to bacterial cellulose nanofibers. Our methodology is based on the use of calibration curves from UV-Vis measurements of solutions of iron (III) chloride in a very specific HCl concentration range (3.7, 4.9, or 9.0 M). Besides, we have determined the minimum time required to ensure the full oxidation of iron (II) to (III) and evaluated the effect of organic interferences by comparing the sample spectra with a master curve for each HCl concentration. Finally, the robustness of each calibration curve and the resulting iron concentration was compared with the values obtained by ICP-OES.

Experimental

Materials

SPIONs were synthesized using iron acetylacetonate (III) (Sigma-Aldrich, 97%) as a metallic precursor and benzyl alcohol (Sharlab, 99%) as an organic solvent. Samples were stabilized in aqueous or in organic media using trisodium citrate dihydrate (Sigma-Aldrich, 99%) and oleic acid (Sigma-Aldrich, 90%), respectively.

For the bacterial cellulose fabrication, the bacterial strain *Komagataeibacter xylinus* (*K. xylinus*) (NCIMB 5346) was purchased from CECT (Valencia, Spain). The culture media were prepared using glucose, peptone, yeast extract and agar (Conda Lab), disodium hydrogen phosphate (Sigma-Aldrich, 99%), and citrate acid monohydrate (Sigma-Aldrich, 99%). For the cleaning process, a solution of 0.1 M of sodium hydroxide (Sigma-Aldrich, ≥ 97%) was used.

For the iron quantification, the following reagents were used as supplied: iron chloride tetrahydrate (II) (Sigma-Aldrich, 98%), iron chloride hexahydrate (III) (Sigma-Aldrich, 99%), hydrochloric acid (Sigma-Aldrich, 37%), and nitric acid (Panreac, 65%). Milli-Q water (MQ-H_2O) was used in all experiments. All materials were used as-received without further purification.

Fabrication of functionalized SPIONs

Samples were obtained by microwave-assisted synthesis (MW) in a CEM Discover reactor (Explorer 12-Hybrid) at a frequency of 2.45 GHz and 300 W of power. Citrate-SPIONs with a mean size of 6 and 9 nm, labeled S6c and S9c, were obtained by following previous reports [20, 21]. Bacterial cellulose nanocomposite containing 7 nm SPIONs (S7bc) and 9 nm oleic acid–coated SPIONs (S9oa) were also produced as previously reported [22, 23].

SPION characterization

Nanoparticle (NP) size and shape were analyzed by using a JEOL JEM-1210 transmission electron microscope operating at 120 KV. Size distributions were obtained by measuring at least 250 NPs and the resultant histograms were fitted to Gaussian functions. NP crystallographic phase was identified by selected area electron diffraction (SAED). Superconductive quantum interference device (SQUID) measurements were recorded on a magnetometer (Quantum Design MPMS5XL) to determine the magnetization of the SPIONs. Hysteresis loops were recorded at 300 K under a maximum field of ± 70 kOe. Saturation magnetization (M_s) values were normalized to the magnetic mass determined by ICP-OES. Zero-field-cooled (ZFC) magnetization curves were measured from 5 to 300 K with a magnetic field of 50 Oe.

Quantification of iron in SPIONs

All the preparations were weighted in an analytic balance with a reproducibility of 0.02 mg ranging from 0 to 50 g to reduce the uncertainty in measurements.

ICP-OES

With ICP-OES, the iron content of samples was determined from the average of two independent solutions with an iron concentration within 15 to 35 mg Fe/l using an ICP-OES Perkin-Elmer Optima 4300DV. Briefly, 100 μl of a citrate-SPION solution was digested in 1 ml of HNO_3 (65%) under sonication for 10 min. After that, the mixture was diluted in a 50-ml volumetric flask with MQ-H_2O. One milligram of S9oa or S7bc was digested in 1 ml of HNO_3 (65%) under 10 min of sonication following a similar procedure. Thereafter, the

sample solution was filtered with a 0.1-μm porous size filter and diluted in a 50-ml volumetric flask with MQ-H_2O.

UV-Vis

UV-Vis spectra were collected on a Varian Cary-5 UV-Vis spectrophotometer from 200 to 800 nm using high-precision cuvettes made of quartz with a light path of 10 mm. Each UV-Vis spectrum was the average of three scans.

Iron calibration curves Twenty milliliters of diluted solutions (DS) of iron (III) chloride with iron concentration ranging from 1.5 to 600 mg Fe/l was prepared by the dilution of one concentrated iron (III) chloride solution using MQ-H_2O. Iron standards for HCl concentrations of 3.7, 4.9, and 9.0 M were made by the controlled addition of HCl (37%) on DS and their later dilution with MQ-H_2O. Iron standards for 3.7 M HCl were done by the addition of 1.5 ml of HCl (37%) on 0.5 ml of DS and the later dilution with 2.5 ml of MQ-H_2O. Iron standards with 4.9 M HCl were carried out mixing 0.5 ml of DS with 2 ml of HCl (37%) and diluted with 2 ml of MQ-H_2O. Finally, 0.5 ml of DS was mixed with 1.5 ml of HCl (37%) for iron standards of 9.0 M HCl. All preparations were stored until used at 4 °C to avoid water evaporation. Each iron calibration curve was obtained by a linear fitting of at least seven points (within the 95% confidence interval) [24]. LOD and LOQ were determined following the next equations:

$$\mathrm{LOD} = (A_{\mathrm{Blank}} + 3\sigma - b)/a \quad (1)$$

$$\mathrm{LOQ} = (A_{\mathrm{Blank}} + 10\sigma - b)/a \quad (2)$$

where A_{Blank} and σ correspond to the average and the standard deviation of 10 absorbance measurements of the blank for each calibration curve. And a and b are respectively the slope and the y-intercept of calibration curve equations [25]. Blanks were prepared for each calibration curve as iron standards but using MQ-H_2O instead of the different DS.

Oxidation kinetics of iron (II) to (III) In total, 3.0 ml of HCl (37%) was added to 1.0 ml of a solution of iron (II) chloride of 64 mg Fe/l and hand-shaken for 10 s. Then, 1.0 ml of the final solution (16 mg Fe/l) was transferred to a UV-Vis cuvette to start the measurement. The UV-Vis spectrophotometer was adjusted to measure automatically every minute, the first 1 h, and every 5 min the following 2 h.

Preparation of sample solutions Sample solutions were prepared in a similar way to the iron standards. The iron content was obtained by the average of two determined iron solutions for each calibration curve. For citrate-SPIONs, 0.5 ml of a diluted solution was mixed with the corresponding volume of HCl (37%) for 1 h and then diluted with MQ-H_2O. Otherwise, 1.0 mg of S9oa or S7bc was mixed in HCl (37%) for 1 h and then filtered with a 0.1-μm porous size filter to remove the organic residues of the sample. Finally, the mixture was diluted for each HCl concentration with MQ-H_2O.

Master curves Master curves for each HCl concentration were obtained as a reference curve of a not interfered absorption profile. Taking into account the reference wavelength (λ_r) used for iron quantification for each HCl concentration, master curves were obtained first normalizing all the UV-spectra obtained with calibration solutions by its absorption at λ_r. Then, all normalized curves were averaged to obtain the final master curve.

Results

Sample characterization

Quantification of iron was performed in SPIONs synthesized by a fast microwave-assisted thermal decomposition method and functionalized with organic molecules following previously reported protocols [19–22]. Figure 1(a–d) displays TEM images for rounded shaped polyhedral particles in different media. Citrate (Fig. 1a–b) and oleic acid–coated (Fig. 1c) samples show SPIONs with an individual particle coating stable in water or organic media respectively. In contrast, Fig. 1d shows SPIONs attached to bacterial cellulose fibers; the particles do not have surface functionalization and are more aggregated. Figure 1(e–h) depicts narrow size distributions for all samples with a mean size of 5.7 ± 0.9 (S6c), 9.4 ± 1.7 (S9c), 9.6 ± 1.4 (S9oa), and 7.1 ± 1.5 nm (S7bc). The crystalline phase was determined by the analysis of the selected area electron diffraction (SAED) patterns (upper insets in Fig. 1(a–d)). Electron diffraction rings for samples were assigned to an inverse spinel structure (γ-Fe_2O_3 or Fe_3O_4). Magnetic characterization techniques revealed the typical features of superparamagnetic behavior. Details of the measurements are described in the experimental part. Hysteresis loops at room temperature did not show remanence and blocking temperatures were ranging from 31 to 100 K in zero-field-cool curves (data not shown) [20–23].

Design of the protocol

Our methodology is based on the complexion of iron with chlorides by the addition of concentrated HCl in iron-containing samples and the controlled dilution of the obtained solutions. The choice of HCl has several justifications. HCl is an economical reagent commonly used to digest iron oxide because of its strong affinity to iron, giving iron chloride complexes with an excellent sensibility in UV-Vis [16–19].

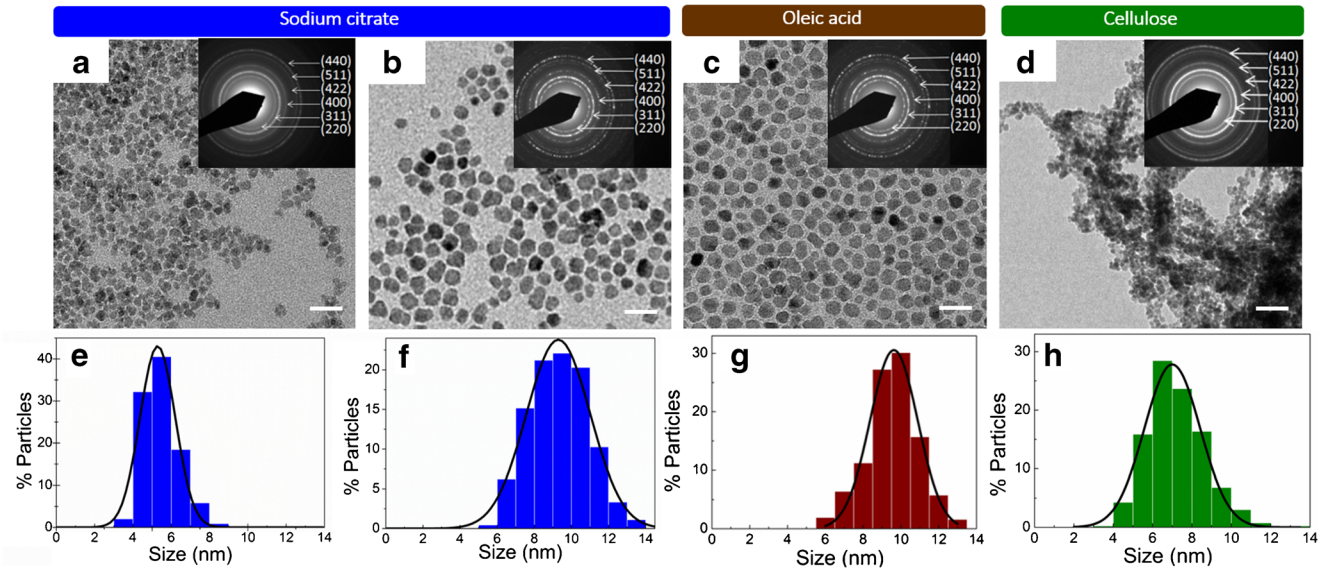

Fig. 1 Structural characterization. TEM images for S6c (**a**), S9c (**b**), S9oa (**c**), and S7bc (**d**). Scale bars are 20 nm in **a**–**c** and 35 nm in **d**. Insets contain a SAED pattern indexed to an inverse spinel structure. Particle size distribution and mean particle were obtained by measuring at least 250 NPs. The resulting histograms were fitted to Gaussian functions for S6c (**e**), S9c (**f**), S9oa (**g**), and S7bc (**h**)

However, HCl concentration has a strong impact on the iron chloride complexes formed (Figure S1) and their different signature in the UV-Vis spectra [16–19]. Figure 2 summarizes this fact by depicting the evolution of the UV-Vis spectra for 0.057 M of $FeCl_3$ and HCl concentrations ranging from 0.20 to 9.0 M. As a general trend, there is an absorbance enhancement together with a shift to lower energies for increasing HCl concentrations. Three types of spectra can be distinguished depending on the HCl concentration. From 0.20 to 4.1 M HCl, the spectra exhibit a single peak around 340 nm associated with $FeCl^{2+}$ and $FeCl_2^{+}$ species [18]. Then, from 4.1 to 5.8 M HCl, a shoulder appears around 315 nm, and the main peak shifts to 355 nm. In this range, $FeCl_3$ is the predominant species giving its absorbance signature [18], with around 80% of the composition of the iron chlorides (Figure S1). The amount of HCl does not affect significantly the reaction equilibrium within this range and the concentration of the species remains stable. Then, for larger HCl concentrations, the spectra exhibit three intense peaks around 250, 315, and 360 nm as the presence of $FeCl_4^{-}$ becomes more important (Figure S1) [18].

As seen above, HCl concentration modifies greatly the UV-Vis response for iron chloride (III) compounds. Slight changes in HCl concentration have a more pronounced effect on the final spectra at low and high HCl concentrations than at moderate ones (4.1–5.8 M HCl), a quasi-stable regime that can help with the experimental uncertainness. However, curves at low HCl concentrations are easy to interpret with one single sharp but less sensitive peak. On the other hand, curves at high HCl concentrations are more sensitive to the iron content but they show multiple peaks that may hinder the interpretation of the results. Thus, the election of an appropriate HCl concentration is crucial for the construction of reliable iron standard calibration curves. In the attempt to shed light on this issue, we have evaluated three different HCl concentrations: 3.7, 4.9, and 9.0 M (one low, one moderate, and one high, respectively), labeled from now on C4, C5, and C9 to ease the reading.

Figure 3 illustrates the steps for the construction of those calibration curves. First, iron standards were made by a controlled addition of HCl (37%) in aliquots of iron (III) chloride with concentrations ranging from 1.5 to 600 mg Fe/l. The final HCl concentration was adjusted with MQ-H_2O (step 1).

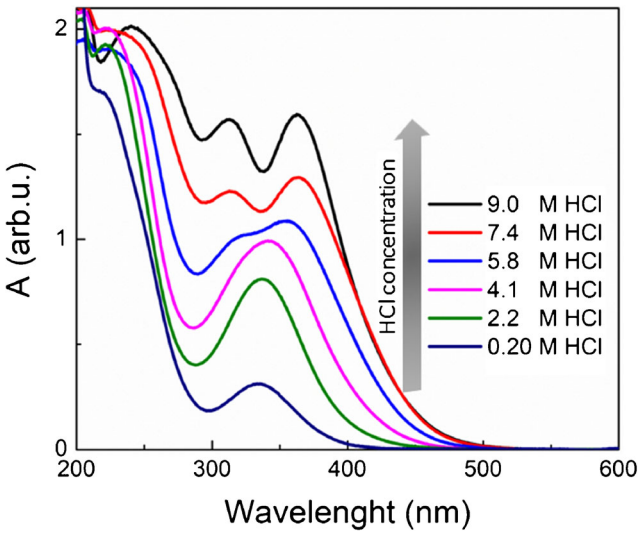

Fig. 2 UV-Vis absorbance spectra for 0.057 M of $FeCl_3$ under HCl concentrations ranging from 0.20 to 9.0 M. Wavelength for each peak as follows: $\lambda_{0.20M} = 335$, $\lambda_{2.2M} = 337$, $\lambda_{4.1M} = 341$, $\lambda_{5.8M} = 355$, $\lambda peak1_{7.4M} = 313$, $\lambda peak2_{7.4M} = 364$, $\lambda peak1_{9.0M} = 241$, $\lambda peak2_{9.0M} = 314$, and $\lambda peak3_{9.0M} = 364$ nm

Afterward, the iron standards were measured by UV-Vis in triplicate and the position of each peak was obtained from the average of these three measurements. Calibration curves were obtained by linear fitting of the maximum peak absorption versus the iron concentration (step 2). Thereafter, we compared the statistical and analytical parameters for each calibration curve. Finally, the reliability for each calibration curve was tested by analyzing iron in various samples containing SPIONs and different surface functionalization. Samples were digested for 1 h to ensure the full iron (II) oxidation and diluted following the same conditions as that of the corresponding standards for each calibration curve (step 3). Then, the iron concentration for each sample was obtained by interpolation in the calibration curve. Simultaneously, ICP-OES sample solutions were prepared by their digestion using concentrated HNO_3 and diluted with MQ-H_2O to the desired volume. Finally, iron concentrations for both methodologies were compared (step 4).

Figure 4 and Table 1 show the main features for C4, C5, and C9 calibration curves. Note that calibration curves were built with at least seven experimental points, which were within the 95% of the confidence interval [24]. They all show an excellent linear response with an $r^2 > 0.997$ [23]. C4 and C5 absorbance curves show a single peak in the range of 340–350 nm, with a linear range within 0.15 to 29 mg Fe/l. In contrast, absorbance curves for C9 depict three peaks ranging from 241 to 364 nm and with a considerable diminution of the linear range, 32% for $\lambda = 314$ and 364 nm, and 62% for 241 nm. The last diminution is caused by the peak position, near the short wavelength limit, in a region prone to spectral interferences due to the multiple UV absorption of chemical species. Besides, the sensibility of each calibration curve was analyzed in terms of the slope of their corresponding linear equation [24], showing greater sensibility for higher HCl concentrations as follows C9 > C5 > C4. Limits of detection (LOD) are within 0.23–0.88 mg Fe/l, while limits of quantification (LOQ) within 0.61–1.4 mg Fe/l.

In Table 1, we summarize the statistical and analytical parameters for both our methodology and other spectroscopic approaches for the iron quantification [11–13, 26, 27]. Note that most studies are based on two steps. First, the addition of an acid to digest the sample and then the generation of UV-Vis quantifiable iron complexes with a medium life of few hours. e.g., methylthymol blue [13], *o*-phenanthroline [26], and Prussian blue [11, 12]. In contrast, our work is based on a single step method where iron is digested generating iron chloride complexes with a sharp signal in the UV-Vis range that is stable for weeks. Besides, greater linear working ranges are found for C4 and C5 absorbance curves of our approach. Finally, our calibration curves show similar values for LOD, LOQ, and r^2 compared with the other spectroscopic methods.

The statistical and analytical parameters from the different standard curves show that the standard curve with the best sensibility is C9 $\lambda = 241$ nm but it has the smaller iron linear range together with slightly higher LOD and LOQ values. The

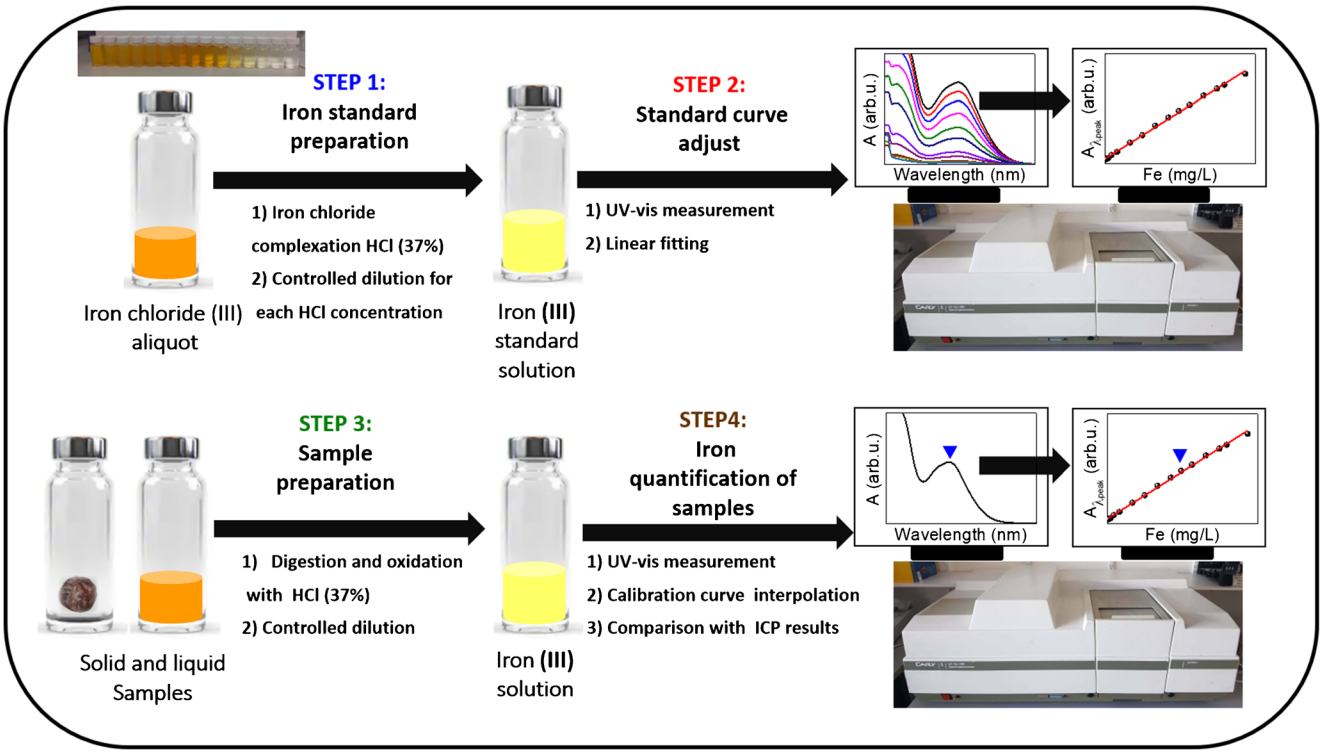

Fig. 3 Schematic illustration for the experimental procedure to quantify iron by a UV-Vis protocol

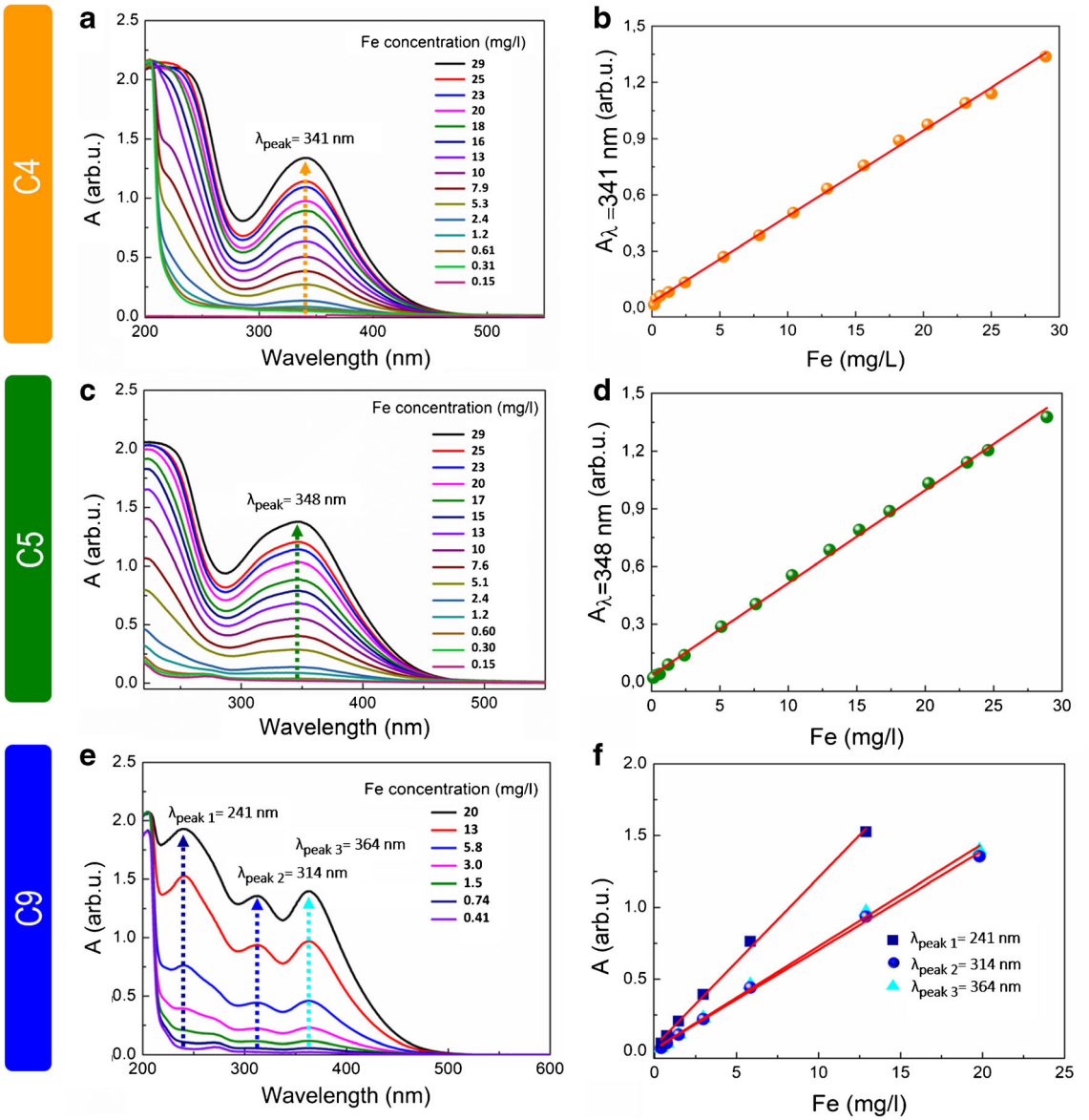

Fig. 4 Construction of the UV-Vis calibration curves. UV-Vis spectra of iron standards with an iron concentration ranging from 0.15 to 29 mg Fe/l for C4 (**a**), C5 (**c**), and C9 (**e**) with a range within 0.41 to 20 mg Fe/l. Iron calibration curves at $\lambda = 341$ nm for C4 (**b**), at $\lambda = 348$ nm for C5 (**d**), and at $\lambda_{peak1} = 241$ nm, $\lambda_{peak2} = 314$ nm, and $\lambda_{peak3} = 364$ nm for C9 (**f**)

opposite trend occurs for C4 and C5. The standard curve with the best combination of sensibility together with greater linear range and low LOD and LOQ values is C5. Thus, C5 is a strong candidate for accurate iron quantification. To validate the robustness of each standard curve and better compare them, C4, C5, and C9 were used for the iron quantification of the sample solutions under study: S6c, S9c, S9oa, and S7bc.

Sample preparation and measurement

All samples were digested using HCl (37%). Since SPIONs can also contain iron (II) if consisting of magnetite (Fe_3O_4), we first determined the minimum time needed for the full oxidation of iron (II) to (III) [28, 29]. Oxidation kinetics was studied by UV-Vis using iron chloride (II) at HCl 9.0 M since this was a higher concentration used to digest the samples (details are included in the experimental section). Figures 5(a, b) shows the evolution of the UV-Vis spectra for 1.0 ml of iron (II) chloride solution (64 mg Fe/l) after the addition of 3.0 ml of HCl (37%). The reaction (final solution of 16 mg Fe/l) was studied comparing the absorbance at $\lambda_{peak}1 = 241$ nm, $\lambda_{peak2} = 314$ nm, and $\lambda_{peak3} = 364$ nm along time up to 100 min. Figure 5b shows the same increase for the three absorbance bands which follows an exponential ($1\text{-}e^{-\alpha t}$) trend. In the first seconds of the reaction, $A_{t=0min} = 0.2\ A_{t=}$

Table 1 Statistical and analytical parameters for C4, C5, and C9 calibration curves (color background rows) and other recent publications (light background rows) in iron quantification spectroscopic techniques. Complexation medium life is in brackets. For the linear fit, y is the absorbance in arbitrary units at the working wavelength and x is the concentration of Fe in mg/l, except that other units are indicated (OD = optical density)

Methodology	λ_{peak} (mn)	Linear fit	r^2	Linear range (mg Fe/l)	LOD (mg Fe/l)	LOQ (mg Fe/l)	Reference
Iron chloride complexes *[several weeks]*	341	y= 0.0460x + 0.0167	0.998	0.15-29	0.23	0.61	*This study (C4)*
Iron chloride complexes *[several weeks]*	348	y= 0.0482x + 0.0320	0.998	0.15-29	0.18	1.2	*This study (C5)*
Iron chloride complexes *[several weeks]*	241 314 364	y= 0.1176x + 0.0321 y= 0.0691x + 0.0135 y= 0.0714x + 0.0149	0.997 0.998 0.997	0.41-13 0.41-20 0.41-20	0.77 0.86 0.88	1.3 1.4 1.4	*This study (C9)*
Methylthymol blue complexation *[90 min]*	628	y= 0.1025x + 0.0013	0.9997	2-6	0.0351	0.1170	*13*
O-phenanthroline complexation (sodium acetate titration) *[several weeks]*	510	y= 0.1969x + 0.0030	0.999972	0-4.6	0.02	-	*26*
O-phenanthroline complexation (in situ 2-nitrophenol pH adjustment) *[several weeks]*	510	y= 0.1963x + 0.0044	0.999988	0-4.6	0.03	-	*26*
Prussian blue *[60 min]*	690	y= 0.0038x + 0.0513	0.9948	0.5-30.0	2.00	-	*11*
SPIONs complexes (ferumoxytol or ferumoxides) *[-]*	370	y= 0.0291x + 0.0052	0.9996	0.2-10.0	-	0.66	*27*
Prussian blue (with comercial SPIONs) *[60 min]*	630	[Fe] (μM)=505.29·OD + 30.18	0.9992	0.22-2.2	-	-	*12*
Prussian blue (with comercial ferric iron solution) *[60 min]*	630	[Fe] (μM)=497.26·OD + 17.22	0.9988	0.625-2.5	-	-	*12*

$_{100min}$, and then increases quickly after 10 min ($A_{t=10min}$ = 0.58 $A_{t=100min}$). After 30 min, the absorbance increases at a slower speed ($A_{t=30min}$ = 0.90 $A_{t=100min}$) and remains constant after 55 min ($A_{t=55min}$ = $A_{t=100min}$). The iron content obtained for $A_{t=60min}$ compares well with that obtained for the calibration curve of iron (III) at the same HCl conditions (Fig. 5c). From these results, we concluded that the minimum time to oxidize iron (II) in our solutions was 60 min.

Next, potential interferences (especially organic interferences, due to the nature of the samples that we used) were evaluated in Figure S2 by comparing the UV-Vis spectra for the sample solutions with the master curves of each HCl concentration. These comparisons do not show appreciable differences in a wide wavelength range around the chosen calibration wavelength. No new peaks appear; neither a shift peak is observed. This obvious coincidence indicates that all iron content is complexed as expected to chloride ions and that no organic or inorganic compounds are absorbing light in the working range. We thus conclude that there are not interferences that could interfere with the iron quantification. However, major differences can be observed in 241 nm case for C9 (Figure S2c), which can be related to the peak position, near the short wavelength limit, in a region prone to spectral interferences due to the multiple UV absorption of chemical species.

Finally, we compared the iron quantification for the studied samples using UV-Vis and ICP-OES. Figure 6 shows this comparison as the mean iron content from the average of

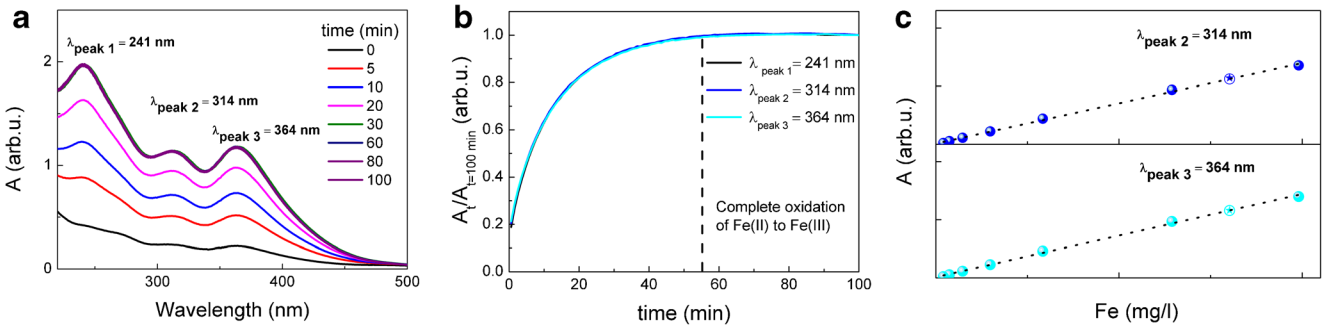

Fig. 5 Oxidation kinetics of iron (II) chloride of 16 mg Fe/l in 9.0 M HCl by UV-Vis. **a** UV-Vis spectra of iron chloride (II) in 9.0 M HCl from 0 to 100 min for selected times. **b** UV-Vis absorbance evolution for each peak as a function of time. **c** Calibration curves at 314 (top) and 364 nm (bottom) for iron (III) chloride in 9.0 M. Stars correspond to values after 60 min of reaction of iron (II) chloride in 9.0 M HCl

two iron dilutions ($[Fe]_{mean}$) for each sample and method with respect to the ICP-OES mean iron content ($[Fe]_{mean,\ ICP\text{-}OES}$). The standard deviation for those values was taken as the half-difference between the two determinations. Error bars in Fig. 6 are given by error propagation of the standard deviations of UV and ICP results to the division. Red dashed lines correspond to differences of ± 5%. All the measurement values and comparisons for each sample and method are detailed in Table S1 in SI.

As a general trend, there is not an influence of the type of sample. Besides, the iron content from ICP-OES shows low dispersity (1–4% in terms of the standard deviation between the two replicates) as expected for this methodology [14, 15]. However, there are large differences in the dispersity of the results depending on the HCl concentration for the UV-Vis approach. The standard curve with the most robust results is C5 showing a dispersity less than 5% and a difference smaller than 5% when compared with ICP-OES results. The C4 standard curve gives values varying ≈ 7% with those obtained from ICP-OES. Finally, the C9 standard curves show two different behaviors depending on the position of the peak. On the one hand, iron values for $C9_{\lambda = 241\ nm}$ have low dispersity comparable with those for C4 and C5 and similar to ICP-OES (except for sample S6c). On the other hand, $C9_{\lambda = 314\ and\ 364\ nm}$ showed higher values of dispersity where the mean iron content differs in more than 10% from the ICP-OES value.

All in all, we concluded that C5 (4.9 M HCl) is the most robust and reliable standard curve for an accurate iron quantification in iron oxide colloids and nanocomposites showing a dispersity of less than 5% between replicates and being comparable with those obtained in ICP-OES as a reference method (with relative errors ranging from 1 to 4%). Indeed, the C5 standard curve was obtained with an HCl concentration placed on the most stable zone on the reaction equilibria of iron (III) chloride compounds (see Figure S1). In this range, the predominant compound is $FeCl_3$ and small variations of HCl concentration coming from the experimental uncertainness have the smallest final impact on the quantification results. Moreover, the use of C5 allows us a suitable compromise between the high sensitivity increasing the HCl concentration and the facile interpretation of the UV-Vis spectra (a single peak observed) decreasing the HCl concentration (Fig. 2), as well as a good statistic and analytical parameters (low LOD and LOQ values and long linear response regime).

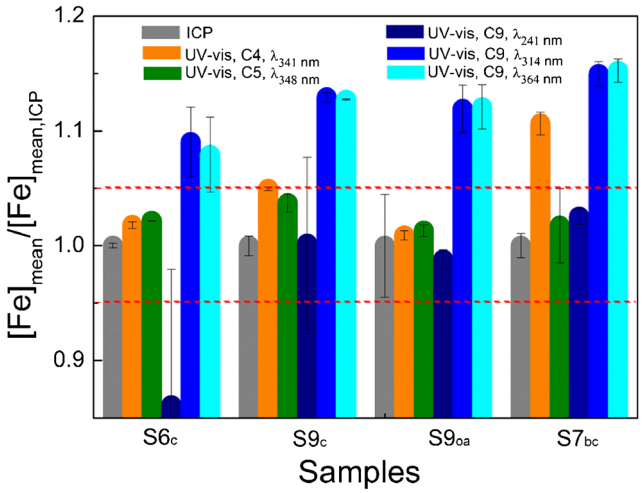

Fig. 6 Comparison of the iron content [Fe] obtained from UV-Vis and ICP-OES analytical techniques. The mean iron content, $[Fe]_{mean}$, for each method as follows: ICP-OES (gray), C4 (orange), C5 (green), $C9_{\lambda 241\ nm}$ (dark blue), $C9_{\lambda 314\ nm}$ (azure blue), and $C9_{\lambda 364 nm}$ (light blue). Error bars correspond to the standard deviation from the average of two iron dilutions for each sample and red dashed lines correspond to differences of ± 5%

Conclusions

By a judicious choice of the methodological conditions, we propose a simple and versatile UV-Vis analytical protocol for an accurate iron quantification in iron oxide samples encompassing SPIONs of different sizes in colloidal dispersion functionalized with widely employed organic molecules (citrate and oleic acid) as well as in a nanocomposite composed of iron oxide nanoparticles decorating bacterial cellulose nanofibers.

To design the protocol, different calibration curves from UV-Vis measurements of solutions of iron (III) chloride under 3.7, 4.9, or 9.0 M HCl were tested (C4, C5, and C9 respectively). All curves showed a good linear response with LOD and LOQ values close to 1 mg Fe/l.

We further determined the minimum time (at HCl 9.0 M) needed for the full oxidation of iron (II) to (III) in the sample concluding that the minimum time to oxidize iron (II) in the solutions studied was 1 h. We then evaluated the effect of interferences by comparing the sample solution spectra with a master curve for each HCl concentration. No new peaks appear in the sample solution spectra that fully overlapped with the mean calibration curves (which we have named here master curves) indicating that the organic coating of the particles does not modify the UV-Vis spectra.

Finally, we compared the iron quantification for the studied samples using both UV-Vis and ICP-OES methods. We concluded that C5, [HCl] = 4.9 M, was the most robust and reliable standard curve for an accurate iron quantification in iron oxide colloids and nanocomposites yielding less than 5% dispersion between replicates and with less than 5% deviation when compared with the values obtained by ICP-OES used here as the "gold standard" method. For this reason, we suggest our C5 UV-Vis analytical protocol as a methodology for an accurate iron determination in iron oxide samples and as an easy-access alternative to ICP-OES.

Acknowledgments The authors thank the Ph.D. students Soledad Roig and Yajie Zhang for helping in the sample fabrication and characterization. The authors would also like to thank Dr Judith Oró from the TEM service at ICMAB.

Funding information This research received funding from the Spanish Ministry of Science, Innovation, and Universities through the PCIN-2017-090 and RTI2018-096273-B-I00, projects and financial support through the Severo Ochoa Programme for Centers of Excelence in R&D (SEV-2015-0496). The Spanish Ministry of Education, Culture and Sport funded the FPU Fellow of M.T. (FPU16/05452). The Argentine National Scientific and Technical Research Council (CONICET) is acknowledged for funding G.A.P. fellowship. Generalitat of Catalunya is acknowledged for the project 2017SGR765. A.R. is grateful for the financial support of Grifols SA with the 2017 Albus Award.

Compliance with ethical standards

Conflict of interest The authors declare that they have no conflict of interest.

References

1. Kandasamy G, Maity D (2015) Recent advances in superparamagnetic iron oxide nanoparticles (SPIONs) for in vitro and in vivo cancer nanotheranostics. Int J Pharm 496:191–218. https://doi.org/10.1016/j.ijpharm.2015.10.058
2. Roca AG, Costo R, Rebolledo AF, Veintemillas-Verdaguer S, Tartaj P, Gonzalez-Carreño T, Morales MP, Serna CJ (2009) Progress in the preparation of magnetic nanoparticles for applications in biomedicine. J Phys D Appl Phys 42(13):224002. https://doi.org/10.1088/0022-3727/42/22/224002
3. Pankhurst QA, Thanh NKT, Jones SK, Dobson J (2003) Progress in applications of magnetic nanoparticles in biomedicine. J Phys D Appl Phys 42:R167–R181. https://doi.org/10.1088/0022-3727/42/22/224001
4. Safarik I, Safarikova M (2004) Magnetic techniques for the isolation and purification of proteins and peptides. Biomagn Res Technol 2:1–17. https://doi.org/10.1186/1477-044X-2-7
5. Laurent S, Saei AA, Behzadi S, Panahifar A, Mahmoudi M (2014) Superparamagnetic iron oxide nanoparticles for delivery of therapeutic agents: opportunities and challenges. Expert Opin Drug Deliv 11:1449–1470. https://doi.org/10.1517/17425247.2014.924501
6. Kallumadil M, Tada M, Nakagawa T, Abe M, Southern P, Pankhurst QA (2009) Structural properties of magnetic nanoparticles determine their heating behavior - an estimation of the in vivo heating potential. JMMM 321:1509–1519. https://doi.org/10.1186/1556-276X-9-602
7. Coral DF, Andrea Soto P, Blank V, Veiga SAE, Gonzalez A, Saracco GP, Bab MA, Muraca D, Setton-Avruj PC, Roig A, Roguin L, Fernández van Raap MB (2018) Nanoclusters of crystallographically aligned nanoparticles for magnetic thermotherapy: aqueous ferrofluid, agarose phantoms and ex vivo melanoma tumour assessment. Nanoscale 10:21262–21274. https://doi.org/10.1039/C8NR07453D
8. Stephen ZR, Kievit FM, Zhang M (2011) Magnetite nanoparticles for medical MR imaging. Mater Today 14:330–338. https://doi.org/10.1016/S1369-7021(11)70163-8
9. Barrow M, Taylor A, Fuentes-Caparrós AM, Sharkey J, Daniels LM, Mandal P, Park K, Murray P, Rosseinsky MJ (2018) In vivo fate of free and encapsulated iron oxide nanoparticles after injection of labelled stem cells. Biomater Sci 6:101–112. https://doi.org/10.1039/C8NA00098K
10. Costo R, Heinke D, Grüttner C, Westphal F, Morales MP, Veintemillas-Verdaguer S, Gehrke N (2018) Improving the reliability of the iron concentration quantification for iron oxide nanoparticle suspensions: a two-institutions study. Anal Bioanal Chem 411:1895–1904. https://doi.org/10.1007/s00216-018-1463-2
11. Maurizi L, Sakulkhu U, Gramoun A, Vallee J-P, Hofmann H (2014) A fast and reproducible method to quantify magnetic nanoparticle biodistribution. Analyst 139:1184–1191. https://doi.org/10.1039/c3an02153j
12. Boutry S, Forge D, Burtea C, Mahieu I, Murariua O, Laurent S, Vander Elsta L, Muller RN (2009) How to quantify iron in an aqueous or biological matrix: a technical note. Contrast Media Mol Imaging 4:299–304. https://doi.org/10.1002/cmmi.291
13. Totan M, Antonescu E, Gligor FG (2018) Quantitative spectrophotometric determinations of Fe^{3+} in Iron Polymaltose solution. Indian J Pharm Sci 80:268–273. https://doi.org/10.4172/pharmaceutical-sciences.1000354
14. Støving C, Jensen H, Gammelgaard B, Stürup S (2013) Development and validation of an ICP-OES method for quantitation of elemental impurities in tablets according to coming US pharmacopeia chapters. J Pharm Biomed Anal 84:209–214. https://doi.org/10.1016/j.jpba.2013.06.007
15. Senila M, Drolc A, Pintar A, Senila L, Levei E (2014) Validation and measurement uncertainty evaluation of the ICP-OES method for the multi-elemental determination of essential and nonessential elements from medicinal plants and their aqueous extracts. J Anal Sci Technol 5:37–45. https://doi.org/10.1186/s40543-014-0037-y
16. Lee MS (2004) Chemical equilibria in ferrous chloride acid solution. Met Mater Int 10:387–392. https://doi.org/10.1007/BF03185990
17. Persson I (2018) Ferric chloride complexes in aqueous solution: an EXAFS study. J Solut Chem 47:797–804. https://doi.org/10.1007/s10953-018-0756-6
18. Liu W, Etschmann B, Brugger J, Spiccia L, Foran G, McInnes B (2006) UV–Vis spectrophotometric and XAFS studies of ferric chloride complexes in hyper-saline LiCl solutions at 25–90 °C. Chem Geol 231:326–334. https://doi.org/10.1007/s10953-018-0756-6
19. Stefansson A, Lemke K, Seward TM (2008) Iron (III) complexation in hydrothermal solutions. An experimental and theoretical study. 15th international conference on the properties of water and steam 15:1-7
20. Yu SM, Laromaine A, Roig A (2014) Enhanced stability of superparamagnetic iron oxide nanoparticles in biological media using a pH adjusted-BSA adsorption protocol. J Nanopart Res 16:2484–2499. https://doi.org/10.1007/s11051-014-2484-1
21. Moya C, Escudero R, Malaspina DC, de la Mata M, Hernández-Saz J, Faraudo J, Roig A (2019) Insights into preformed HSA corona on iron oxide nanoparticles: structure, effect of particle size, impact on MRI efficiency and metabolization. ACS Appl Bio Mater 2:3084–3094. https://doi.org/10.1021/acsabm.9b00386
22. Zhang Y, García-Gabilondo M, Grayston A, Feiner IVJ, Anton-Sales I, Llop J, Ramos-Cabrer P, Barba I, Loiola RA, Garcia-Dorado D, Gosselet F, Rosell A, Roig A (2020) In vivo studies of PLGA nanocapsules as a drug delivery platform with made-to-order multimodal imaging modalities. Nanoscale 12:4988–5003. https://doi.org/10.1039/C9NR10620K
23. Roig-Sanchez S, Jungstedt E, Anton-Sales I, Malaspina DC, Faraudo J, Berglund LA, Laromaine A, Roig A (2019) Nanocellulose films with multiple functional nanoparticles in confined spatial distribution. Nanoscale Horizons 4:634–641. https://doi.org/10.1039/C8NH00310F

24. Meier PC, Zünd RE (2000) Statistical methods in analytical chemistry, 2nd edn. https://doi.org/10.1002/0471728411
25. McNaught AD (1997) Wilkinson a (1997) IUPAC compendium of chemical terminology, 2nd edition (the "gold book"), vol 39. Scientific Publications, Oxford, p 150. https://doi.org/10.1002/actp.1988.010390322
26. Serra-Mora P, Moliner-Martínez Y, Herráez-Hernández R, Verdú-Andrés J, Campíns-Falcó P (2016) Simplifying Iron determination with o-Phenanthroline in food ashes using 2-Nitrophenol as an Acid-Base indicator. Food Anal Methods 9:1150–1154. https://doi.org/10.1007/s12161-015-0294-4
27. Dadashzadeha ER, Hobsona M, Bryant LH Jr, Deana DD, Frank JA (2013) Rapid spectrophotometric technique for quantifying iron in cells labeled with superparamagnetic iron oxide nanoparticles: potential translation to the clinic. Contrast Media Mol Imaging 8: 50–56. https://doi.org/10.1002/cmmi.1493
28. Posner AM (1953) The kinetics of autoxidation of ferrous ions in concentrated HCl solutions. Trans Faraday Soc 49:382–388. https://doi.org/10.1039/TF9534900382
29. Porsch K, Kappler A (2011) Fe^{II} oxidation by molecular O_2 during HCl extraction. Environ Chem 8:190–197. https://doi.org/10.1071/EN10125